

# Electrogyration in Metamaterials: Chirality and Polarization Rotatory Power that Depend on Applied Electric Field

Qiang Zhang, Eric Plum,\* Jun-Yu Ou, Hailong Pi, Junqing Li,\* Kevin F. MacDonald,\* and Nikolay I. Zheludev\*

One of the most fascinating properties of chiral molecules is their ability to rotate the polarization of light. Since Faraday's experiments in 1845, it has been known that nonreciprocal polarization rotatory power can be induced by a magnetic field. But can reciprocal polarization rotation in chiral molecules be influenced by an electric field? In the 1960s, Aizu and Zheludev introduced the phenomenon of electrogyration. While the linear (Pockels) and quadratic (Kerr) electro-optical effects describe how an external electric field changes linear birefringence and dichroism, electrogyration describes how a field changes the circular birefringence and dichroism of a medium. Electrogyration is observed in dielectrics, semiconductors, and ferroelectrics, but the effect is small. This work demonstrates a nanostructured photonic metamaterial that exhibits quadratic electrogyration—proportional to the square of the applied electric field—six orders of magnitude stronger than in any natural medium. Giant quadratic electrogyration emerges as electrostatic forces acting against forces of elasticity change the chiral configuration of the metamaterial's nanoscale building blocks and consequently its polarization rotatory power. This observation of giant electrogyration alters the perception of the effect from that of an esoteric phenomenon into a functional part of the electro-optic toolkit with application potential.

## 1. Introduction

Optical activity manifests itself as circular birefringence—rotation of the polarization state of light, and circular dichroism—differential transmission of circularly polarized waves. Over 200 years have passed since the discovery of optical activity by Arago, and it is now well-understood that the effect is linked to chirality, i.e., to structures or experiments that are different from their mirror image. In 1845, Faraday discovered that optical activity can be changed by an external magnetic field, but it took another 117 years until the electrical counterpart of the Faraday effect was found in ferroelectric crystals, where optical activity was changed by an external electric field.<sup>[1]</sup> At around the same time, Aizu and Zheludev independently described this phenomenon, naming it the gyroelectric effect or electrogyration.<sup>[2,3]</sup> The Faraday effect is nonreciprocal, i.e., the optical rotation continues to grow

when the wave's propagation direction is reversed. In contrast, optical activity and electrogyration are reciprocal, i.e., optical rotation is compensated upon reversal of the propagation direction. Electrogyratory polarization changes that depend linearly on electric field have been reported for crystals of various point symmetry groups,<sup>[4]</sup> and quadratic electrogyration has been observed in crystalline quartz and tellurium dioxide.<sup>[5,6]</sup>

As electrogyration is weak in natural materials, anticipation has been growing that a stronger effect might be engineered in artificial chiral metamaterials.<sup>[7]</sup> Many chiral metamaterials have been shown to exhibit optical activity exceeding that of natural materials by several orders of magnitude, but the complex geometry of these typically 3D structures makes fabrication of chiral metamaterials for the optical part of the spectrum challenging,<sup>[8–15]</sup> and has limited their realization. Indeed, most 3D-chiral metamaterials, especially those with controllable chirality, are designed for terahertz and microwave radiation.<sup>[16–20]</sup> Planar chiral patterns (e.g., flat spirals) form 3D-chiral structures with a supporting substrate, and are relatively easy to fabricate, but the resulting optical activity is typically weak.<sup>[21]</sup> Reconfigurable nanomembrane metamaterials provide an extra degree of freedom for controlling structures:<sup>[22]</sup> Actuation by electromagnetic Coulomb, Lorentz, Ampère, or optical forces as well as thermal stimulation can provide dynamic control over the optical properties of reconfigurable

Dr. Q. Zhang, Dr. E. Plum, Dr. J.-Y. Ou, Prof. K. F. MacDonald, Prof. N. I. Zheludev  
Optoelectronics Research Centre and Centre for Photonic Metamaterials  
University of Southampton  
Southampton SO17 1BJ, UK  
E-mail: erp@orc.soton.ac.uk; kfm@orc.soton.ac.uk; niz@orc.soton.ac.uk

Dr. Q. Zhang, Prof. J. Li  
School of Physics  
Harbin Institute of Technology  
92 Western Dazhi, Harbin 150001, China  
E-mail: jqli@hit.edu.cn

H. Pi  
School of Electronics and Computer Science  
University of Southampton  
Southampton SO17 1BJ, UK

Prof. N. I. Zheludev  
Centre for Disruptive Photonic Technologies SPMS, TPI,  
Nanyang Technological University  
Singapore 637371, Singapore

 The ORCID identification number(s) for the author(s) of this article can be found under <https://doi.org/10.1002/adom.202001826>.

© 2020 The Authors. Advanced Optical Materials published by Wiley-VCH GmbH. This is an open access article under the terms of the Creative Commons Attribution License, which permits use, distribution and reproduction in any medium, provided the original work is properly cited.

DOI: 10.1002/adom.202001826

metamaterials<sup>[16,23–32]</sup> and has enabled demonstrations of giant electro-optic, magneto-electro-optic, nonlinear optical, and thermo-optic effects.

Here, we report on the observation of giant electrogyration in the optical part of the spectrum. An applied electric field reversibly controls the optical activity of a photonic metamaterial of nanoscale thickness, providing a 16° range of azimuth rotation and a 9° range of ellipticity angle change for transmitted near-infrared light. This change of optical activity results from electrostatic forces (between the metamaterial and a transparent electrode) that control the metamaterial's chirality via nanoscale reconfiguration of its constituent components. The effect is quadratically dependent on electric field and a million times stronger than in naturally occurring materials. Our results also suggest the emergence of higher-order electrogyration at larger applied fields.

## 2. Results

### 2.1. Local and Nonlocal Electro-Optic Effects

Following ref. [33], in linear optics, the electric field displacement  $D(\omega)$  induced in a medium by a light wave  $E(\omega)$  with frequency  $\omega$  and wave vector  $k$  is given by the constitutive equation

$$D_i^{(1)}(\omega) = \varepsilon_{ij}(\omega) \times E_j(\omega) + i k_l \Gamma_{ijl}(\omega) \times E_j(\omega) \quad (1)$$

Here, the local optical properties of the medium, including absorption, refraction, linear birefringence, and linear dichroism, are described by the frequency-dependent symmetric second rank dielectric tensor  $\varepsilon_{ij}(\omega) = \varepsilon_{ji}(\omega)$ . First-order nonlocal effects such as circular birefringence and circular dichroism are introduced by the third rank nonlocality tensor, which is antisymmetric in relation to its first two indices (i.e.,  $\Gamma_{ijl}(\omega) = -\Gamma_{jil}(\omega)$ ).

In a static electric field  $E(0)$ , the total displacement in a medium includes power expansion terms in the static field

$$D_i(\omega) = D_i^{(1)}(\omega) + D_i^{(2)}(\omega) + D_i^{(3)}(\omega) + \dots \quad (2)$$

where

$$D_i^{(2)}(\omega) = 2\chi_{ijl}^{(2)}(\omega, \omega, 0) \times E_j(\omega) E_l(0) + i k_m \Gamma_{ijlm}^{(2)}(\omega, \omega, 0) \times E_j(\omega) E_l(0) \quad (3)$$

and

$$D_i^{(3)}(\omega) = 3\chi_{ijlm}^{(3)}(\omega, \omega, 0, 0) \times E_j(\omega) E_l(0) E_m(0) + i k_n \Gamma_{ijlmn}^{(3)}(\omega, \omega, 0, 0) \times E_j(\omega) E_l(0) E_m(0) \quad (4)$$

Here, the third rank tensor  $\chi_{ijl}^{(2)}(\omega, \omega, 0)$  describes the linear electro-optic (Pockels) effect, whereas the fourth rank tensor  $\chi_{ijlm}^{(3)}(\omega, \omega, 0, 0)$  describes quadratic changes to linear birefringence and dichroism—the quadratic electro-optic (Kerr) effect. The dependence of circular birefringence and dichroism on the first power of external static electric field is introduced by

the fourth rank tensor  $\Gamma_{ijlm}^{(2)}(\omega, \omega, 0)$ , whereas quadratic terms in the dependence are introduced by the fifth rank tensor  $\Gamma_{ijlmn}^{(3)}(\omega, \omega, 0, 0)$ .

It should be noted that changes to linear and circular birefringence and dichroism that are quadratic in electric field can also be induced by an intense light beam itself and are described by a similar constitutive equation

$$D_i^{(3)}(\omega) = 3\chi_{ijlm}^{(3)}(\omega, \omega, \omega, -\omega) \times E_j(\omega) E_l(\omega) E_m^*(\omega) + i k_n \Gamma_{ijlmn}^{(3)}(\omega, \omega, \omega, -\omega) \times E_j(\omega) E_l(\omega) E_m^*(\omega) \quad (5)$$

where the tensor  $\chi_{ijlm}^{(3)}(\omega, \omega, \omega, -\omega)$  describes the quadratic Stark effect, and the tensor  $\Gamma_{ijlmn}^{(3)}(\omega, \omega, \omega, -\omega)$  describes the phenomenon of nonlinear optical activity.

Circular birefringence gives rise to rotation of the polarization state of light where the angle of rotation  $\Delta\varphi$  of light propagating along the  $z$ -direction with a static electric field applied along the  $z$ -direction is proportional to the thickness of the sample  $L$

$$\Delta\varphi = \frac{\omega^2}{2c^2} \text{Re} \left\{ \Gamma_{xyz}(\omega) + \Gamma_{xyz}^{(2)} E_z(0) + \Gamma_{xyz}^{(3)} E_z(0) E_z(0) \right\} L \quad (6)$$

Earlier sources introduce an expansion of the gyration tensor in the static electric field<sup>[4]</sup>

$$g_{ij} = g_{ij}^{(0)} + \gamma_{ijl} E_l + \beta_{ijlm} E_l E_m + \dots \quad (7)$$

where, in relation to the constitutive equations of the medium,  $g_{ij}^{(0)} = k_l \Gamma_{ijl}(\omega)$ ,  $\gamma_{ijl} = k_m \Gamma_{ijlm}^{(2)}(\omega, \omega, 0)$ , and  $\beta_{ijlm} = k_n \Gamma_{ijlmn}^{(3)}(\omega, \omega, 0, 0)$ . In this work, we engineer a metamaterial where the latter term for quadratic electrogyration is exceptionally large.

### 2.2. Design of Electrogyratory Metamaterial

The metamaterial comprises a periodic array of patterned nanowires manufactured on a freestanding 100-nm-thick silicon nitride membrane coated with 50 nm of gold (see the Experimental Section). Nanowires with length 37  $\mu\text{m}$  and width  $w = 500$  nm, separated by gaps of  $d = 170$  nm, were chosen to facilitate mutual displacement (length), while preventing them from touching (gaps) and enabling a nondiffracting metamaterial structure (width). Each nanowire is perforated with alternating large and small semicircular notches with radii  $R_{1,2} = 260$  and 120 nm, as illustrated in Figure 1c,d. The structure has periodic unit cell dimensions  $P_{x,y} = 1340$  and 1370 nm chosen to avoid diffraction at experimental wavelengths above 1370 nm. The sizes and positions of notches on neighboring beams are chosen to form a simplified planar (2D) spiral-like hole, which can be deformed into a 3D helix-like geometry by their mutual out-of-plane displacement. To facilitate such movement, the ends of the beams—their connection points to the surrounding (unstructured) membrane—are patterned to endow neighboring beams with alternating mechanical and electrical properties: Mechanical flexibility is enhanced [inhibited] by narrowing [widening] the beam toward the ends

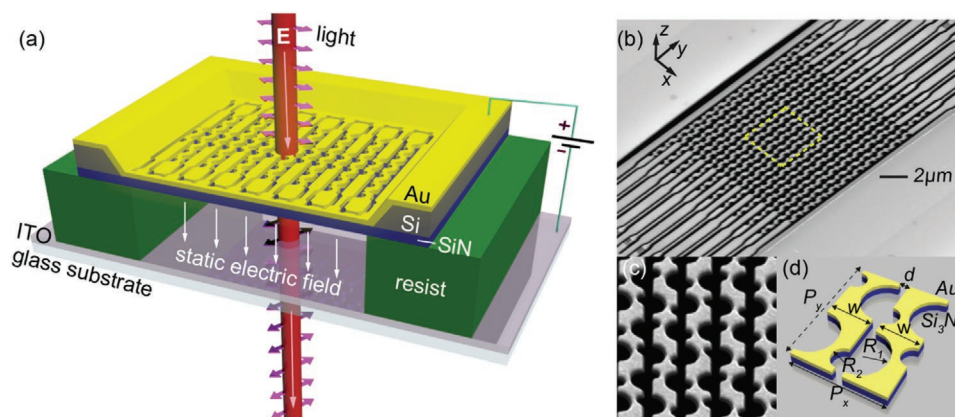


**Figure 1.** Electrogyratory metamaterial. a) Artistic impression of the metamaterial, consisting of a nanostructured gold-coated silicon nitride membrane, suspended above an ITO-coated glass back-plane. Static electric field actuates the nanomechanical material, changing its chirality and optical activity. b,c) Scanning electron microscope (SEM) images of the metamaterial. d) Dimensional schematic of the metamaterial unit cell:  $P_{x,y} = 1340, 1370$  nm,  $w = 500$  nm,  $d = 170$  nm, and  $R_{1,2} = 260, 120$  nm.

and by extending [limiting the extent] of the notch pattern along the beam, in the  $y$ -direction; electrical isolation of every other beam is achieved by cutting a trench through the gold layer at either end, close to the anchor points (see detail of the gold layer at top-right and bottom-left of the scanning electron microscope [SEM] image in Figure 1b).

The metamaterial is suspended above a grounded transparent indium tin oxide (ITO) back-plane at a distance of about  $4 \mu\text{m}$ , as shown in Figure 1a, such that the application of a bias voltage between the gold and ITO electrode layers leads to charge accumulation in the metamaterial, enabling electrostatic reconfiguration of its structure.<sup>[34,35]</sup> Electrically connected beams deform (bend toward the back-plane) under the action of the applied electrostatic force, to a point where this force is balanced by the elastic restoring force generated within the beam. Electrically isolated beams do not accumulate charge, are consequently not subject to an electrostatic force, and therefore do not move. An applied voltage thus controls the metamaterial's chirality and optical activity by controlling the relative ( $z$ -direction) displacement of the beams that make up the metamaterial structure.

The metamaterial is achiral when flat, with all beams in the same plane. Figure 2a demonstrates this by showing how a unit cell of the metamaterial in its planar (2D) state can be superimposed on its mirror image by a simple half-period translation in both the  $x$  and  $y$ -directions. The same can also be understood by considering that the pairs of large and small semicircular notches on adjacent beams form flat spirals with alternating senses of twist (each unit cell contains two left- and two right-handed spirals). However, when alternate beams are mutually displaced in the  $z$ -direction these planar spirals are transformed into 3D helices all having the same sense of twist, i.e., such that a unit cell contains either four left- or four right-handed helices, depending upon the direction of mutual beam displacement. This is illustrated in Figure 2b,c, where superimposed red helical lines connecting the arcs of paired semicircular notches are extended to two full turns to more clearly reveal their handedness. The magnitude of applied voltage (electrostatic force) controls the magnitude of beam displacement, which is

proportional to the pitch of the helices, and will therefore control the magnitude of optical activity.

### 2.3. Observation of Electrogyration

On propagation through a chiral medium, a wave with initially linear polarization becomes elliptically polarized and its polarization azimuth rotates. Figure 3 shows measurements of the voltage-dependent spectral dispersion of these polarization changes for transmission through the metamaterial of normally incident light polarized perpendicular to the beams of the structure. In the absence of an applied field (i.e., at 0 V bias) the metamaterial exhibits moderate azimuth rotation  $\Delta\varphi$  [panel (a)] and ellipticity angle change  $\Delta\zeta$  [panel (b)], not exceeding  $6^\circ$  in either case. These are a consequence of the fact that in practice the metamaterial is not perfectly flat (and therefore achiral) in its zero-bias state: Small systematic mutual displacements between neighboring beams exist in the fabricated nanostructure because of the differing strengths of the widened- and narrowed-end beam anchor points and the electrical isolation trenches (a break in the gold relieves stress between the metal and dielectric layers). With increasing applied electrical bias the polarization state of transmitted light changes at an increasing rate: Relatively little change is seen between 0 and 10 V, but by 18 V azimuth rotation reaches  $-13.3^\circ$  and  $+22.7^\circ$  at wavelengths of 1520 and 1600 nm, respectively, and ellipticity reaches  $-23.9^\circ$  at an intermediate wavelength of 1560 nm. We note that the spectral positions of both the largest positive azimuth rotation and largest negative ellipticity change blueshift with increasing bias. When recording the measurement series of Figure 3, voltage was turned on and off at each combination of voltage and wavelength, i.e., the data correspond to 360 on/off cycles of voltage application over a period of about 8 h. A second complete measurement cycle (see Figure S1, Supporting Information) reproduces the data in Figure 3a with an average deviation of only  $0.2^\circ$  azimuth rotation, indicating that repeated cycles of voltage application do not cause any significant permanent changes. Numerical simulations show that the magnitude of

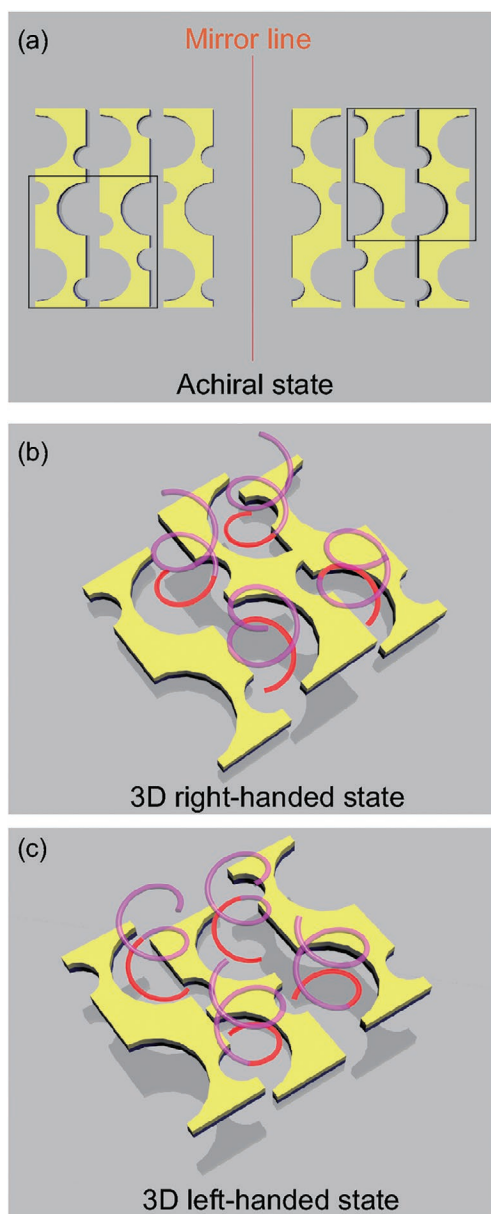


**Figure 2.** The origin of tunable metamaterial chirality. a) The structure is achiral when the metamaterial beams all lie in the same plane. In this case, the metamaterial (left) and its mirror image (right) have identical unit cells (rectangular box). b, c) With mutual out-of-plane displacement between alternate beams, either right-handed or left-handed chirality emerges, depending upon the direction of said displacement. In each case, the semicircular notches all form simplified helix-like geometries of the same, left or right, handedness. To aid visualization, helices are superimposed in red and extended over two full turns in purple.

the observed effect is consistent with relative nanowire displacements of up to  $\sim 300$  nm (see Figure S2, Supporting Information).

In general, in media with low symmetry, chirality coexists with anisotropy. The latter manifests itself as differential refraction (birefringence) and transmission (dichroism) for orthogonal linear polarizations. As in chiral media, waves with initially linear polarization become elliptically polarized with rotated polarization azimuth on propagation through anisotropic media.

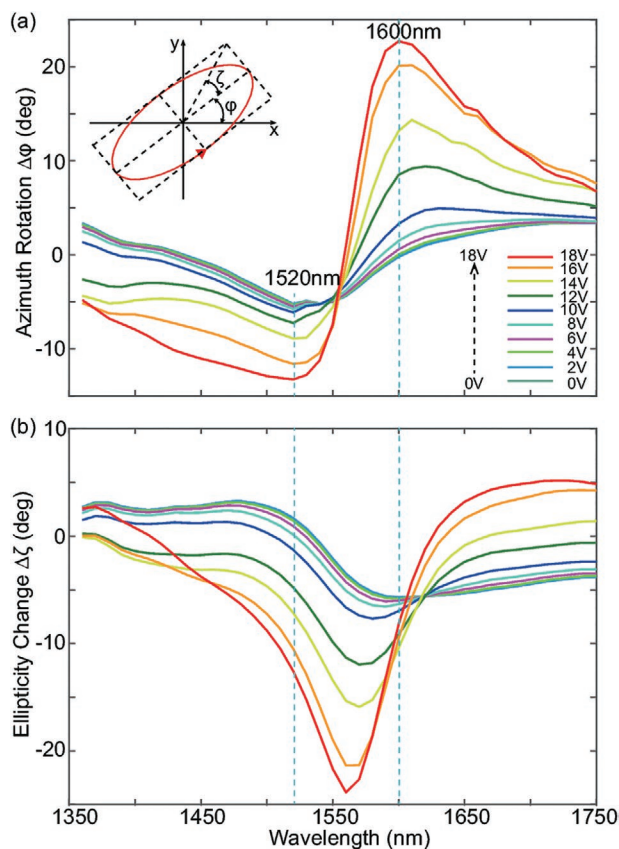


**Figure 3.** Control of polarization azimuth and ellipticity by electric field. Spectral dispersion of a) azimuth rotation  $\Delta\phi$  and b) ellipticity angle change  $\Delta\zeta$  for normally incident x-polarized light at a selection of different applied static bias levels from 0 to 18 V. The inset defines azimuth and ellipticity angles with respect to the metamaterial coordinate frame introduced in Figure 1b.

It is therefore necessary to distinguish between polarization changes because of chirality and anisotropy. In contrast to those associated with optical activity, polarization changes derived from anisotropy are inherently linked to certain directions in the material coordinate frame. As such, their magnitude oscillates as a function of the incident wave's polarization azimuth. Optical activity in anisotropic media thereby corresponds to the component of polarization change that does not oscillate with incident azimuth and can be evaluated as the average polarization change over all incident azimuth orientations. So, to quantify the metamaterial's optical activity in the present case, we evaluated the transmitted beam's azimuth rotation and ellipticity for linearly polarized incident light with azimuthal angles ranging from  $0^\circ$  to  $180^\circ$  in  $15^\circ$  steps, at wavelengths of 1520 and 1600 nm (i.e., those of maximum observed positive and negative azimuth rotation, identified in Figure 3a).

The bias voltage dependence of metamaterial optical activity, in terms of circular birefringence and dichroism (i.e., azimuth and ellipticity angle change averaged over incident polarization azimuth), is then plotted in Figure 4. Again, we note here that (for the reasons discussed above) optical activity is not zero at zero bias. However, circular birefringence and dichroism at both wavelengths go to zero at 8 V, indicating that the field-induced

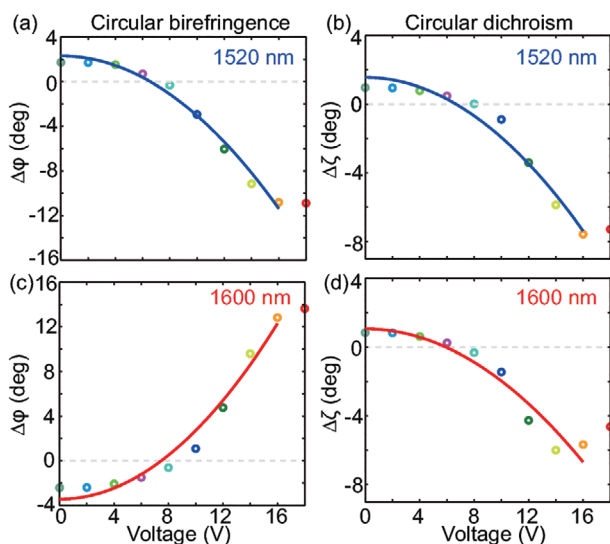


**Figure 4.** Giant electrogyration. Dependences on applied bias of the metamaterial's a,c) circular birefringence in terms of average polarization azimuth rotation  $\Delta\phi$  and b,d) circular dichroism in terms of average ellipticity angle for transmission of normally incident linearly polarized light at wavelengths of (a, b) 1520 nm and (c, d) 1600 nm. Data points are experimental results with colors corresponding to applied bias levels as in the curves of Figure 3. Lines show quadratic fits from 0 to 16 V. (Figure S3, Supporting Information, shows these results in terms of Stokes parameters.)

deformation of the structure at this bias setting compensates for the initial relative displacement offset between neighboring nanowires, bringing the metamaterial close to its planar achiral state. This in turn implies that the handedness of the structure changes as the applied bias crosses the 8 V level. This is confirmed by changes in the sign of both circular birefringence and circular dichroism at both measurement wavelengths. Both circular birefringence and circular dichroism exhibit a nonlinear dependence on applied bias voltage, approximated as quadratic at low voltage, but saturating as the applied bias approaches 18 V. This empirical saturation voltage is determined by the device geometry and intrinsic material properties, and from simulations corresponds to mutual nanowire displacement approaching 400 nm (Figure S2, Supporting Information).

Numerical simulations reveal a complex metamaterial response to circularly polarized light, which is characterized by electromagnetic coupling between the nanowires and charge accumulation at their edges. Without nanowire displacement, the structure is achiral and the modes excited by left- and right-handed circularly polarized waves (LCP and RCP) have glide mirror symmetry. Upon nanowire displacement, this symmetry vanishes, the structure becomes 3D-chiral, and the modes excited by LCP and RCP become distinctively different, resulting in optical activity of the nanostructure (see Figure S4, Supporting Information).

### 3. Discussion

For comparison of our metamaterial to natural materials, we estimate the magnitude of the relevant tensor components from the observed electric-field-dependent optical activity. In

our experimental configuration, both the propagation direction of the incident wave and the applied electric field are oriented along the  $z$ -direction. Optical activity without application of external field would be zero for a perfectly flat structure (Figure 2a). However, a small zero-bias displacement of neighboring beams makes our fabricated metamaterial optically active as discussed above, i.e.,  $\Gamma_{xyz} \neq 0$ . Application of electric field yields additional deformation of the nanomechanical metamaterial. As electrostatic forces between opposite charges are always attractive, application of positive or negative electrical bias necessarily generates the same pulling force on components of the metamaterial. Therefore, the voltage dependence of both deformation and associated optical properties must be symmetric around 0 V. It follows that a Taylor expansion of the metamaterial's optical activity in electric field  $E_z$  can only include even terms proportional to  $E_z^0$  (optical activity),  $E_z^2$  (quadratic electrogyration),  $E_z^4$ , etc. In particular, linear electrogyration cannot occur ( $\Gamma_{xyzz}^{(2)} = 0$ ) as it is proportional to  $E_z^1$ , but quadratic electrogyration is allowed ( $\Gamma_{xyzz}^{(3)} \neq 0$ ). Indeed, quadratic electrogyration is to be expected considering that the attractive electrostatic forces in the similar geometry of a parallel plate capacitor depend quadratically on voltage (electric field).

Consider the measured voltage dependence of circular birefringence at a wavelength of 1600 nm (Figure 4c). In the absence of an applied voltage, the metamaterial layer of  $L \approx 150$  nm thickness rotates the polarization state of the incident wave by  $\Delta\phi_0 = -2.4^\circ$ , corresponding to a rotatory power of  $-16000^\circ \text{ mm}^{-1}$ , nonlocality of  $\text{Re}(\Gamma_{xyz}) = \frac{2c^2 \Delta\phi_0}{\omega^2 L} = -4 \times 10^8 \text{ rad m}$  and gyration of  $\text{Re}(g_{xy}^{(0)}) = -0.2 \text{ rad}$ . Gyration is calculated as the product of nonlocality and wave vector, taking into account the metamaterial's effective refractive index of 1.4 (evaluated following ref. [36]).

Polarization rotation in the metamaterial changes by  $\Delta\phi_2$  in response to electric field  $E = U/h$  generated along the propagation direction by applying bias voltage  $U$  across the  $h \approx 4 \mu\text{m}$  capacitive gap between metamaterial and ground plane. (Saturation effects emerge above 16 V, suggesting that higher-than-quadratic even-order contributions may play an increasing role in this regime.) According to the fit in Figure 4c,  $\frac{\Delta\phi_2}{E^2} \approx 1.7 \times 10^{-14} \text{ rad m}^2 \text{ V}^{-2}$ , and in the small-displacement limit where  $L \approx 150$  nm, the corresponding nonlocality tensor component  $\Gamma_{xyzz}^{(3)} = \frac{2c^2 \Delta\phi_2}{\omega^2 L E^2} \approx 1.5 \times 10^{-20} \text{ rad m}^3 \text{ V}^{-2}$  is equivalent to quadratic electrogyration of  $\text{Re}(\beta_{xyzz}) \approx 8.2 \times 10^{-14} \text{ rad m}^2 \text{ V}^{-2}$ . This is a million times stronger than in natural materials known to exhibit quadratic electrogyration (e.g., quartz:  $4.5 \times 10^{-20} \text{ rad m}^2 \text{ V}^{-2}$ , tellurium dioxide:  $6.6 \times 10^{-20} \text{ rad m}^2 \text{ V}^{-2}$ ).<sup>[6]</sup> Electrogyration in natural materials as well as the metamaterial results from a perturbation of the material in response to applied electric field. However, the metamaterial is designed to achieve significant mechanical perturbations that control its chirality, resulting in a much bigger electrogyration effect.

We note that statically prepolarized metamaterials will also exhibit linear electrogyration (and possibly higher-than-linear odd-order contributions) if the applied external electric field competes with the internal static field. For instance, this can be

achieved by a metamaterial consisting of both a nanostructured membrane and a statically charged electrode, or by inserting a prepolarized transparent ferroelectric layer as a part of the structure.

The giant quadratic electrogyration effect reported here resembles the phenomenon of nonlinear optical activity, the dependence of the rotatory power on light's intensity. Indeed, quadratic electrogyration is described by  $\Gamma_{ijlmn}^{(3)}(\omega, \omega, 0, -0)$  and nonlinear optical activity is described by  $\Gamma_{ijlmn}^{(3)}(\omega, \omega, \omega, -\omega)$  (see constitutive equations above). In the electrogyration effect, the square of static electric field matters, whereas in nonlinear optical activity it is the square of optical field that matters, i.e., light intensity. Nonlinear optical activity is also very weak in natural media,<sup>[37]</sup> whereas purposely designed optical metamaterials show a seven orders of magnitude stronger effect,<sup>[38]</sup> and in microwave chiral structures the effect is 12 orders of magnitude stronger.<sup>[39]</sup>

## 4. Conclusion

In summary, we demonstrate a metamaterial where optical activity is controlled by electric field. We observe quadratic electrogyration that is more than six orders of magnitude larger than has been observed in natural materials. This optical phenomenon is achieved by engineering the chiral properties of a nanomechanical metamaterial, which is actuated by electrostatic forces. Dynamic ranges of 16° azimuth rotation and 9° ellipticity angle in a metamaterial of nanoscale thickness transform electrogyration from being an obscure effect of only academic interest into a phenomenon with potential for practical application. Metamaterial nanomechanical chirality modulators could find applications in integrated photonic chips, compact dichroic spectrometers, and other nanophotonic devices.

## 5. Experimental Section

**Metadevice Fabrication:** The metamaterial sample was manufactured on a 100-nm-thick  $0.5 \times 0.5 \text{ mm}^2$  silicon nitride membrane supported by a 200- $\mu\text{m}$ -thick  $5 \times 5 \text{ mm}^2$  silicon frame. The back side of the membrane and frame was coated with 50 nm of gold by thermal evaporation. The metamaterial array of nanowire pairs with semicircular notches was fabricated by focused ion beam milling from the gold-coated side of the bilayer, cutting through both layers of material.

For the back-plane of the device, a 0.5-mm-thick glass substrate was coated with 50 nm of ITO from  $\text{In}_2\text{O}_3/\text{SnO}_2$  (90/10 wt%) alloy pellets by electron beam evaporation. A base pressure of  $5 \times 10^{-6}$  mbar was achieved before deposition. An oxygen pressure of  $1.5 \times 10^{-4}$  mbar was maintained in the chamber during deposition. The ITO layer was subsequently annealed at 280 °C for 3 h under an oxygen atmosphere to increase conductivity and transparency—sheet resistance was subsequently evaluated in a four-point probe measurement as  $60 \Omega \text{ sq}^{-1}$ . The ITO film was then spin-coated with S1813 photoresist and baked at 120 °C for 1 min. The final device comprises the nanostructured membrane separated by the photoresist from the ITO-coated glass substrate, which forms a capacitor configuration. A channel of  $\approx 1$  mm width defined in the resist by photolithography ensures that the nanomechanical metamaterial remains free to move in the assembled device. The size of the air gap between the metamaterial and the ITO back-plane was determined to be  $\approx 4 \mu\text{m}$  based on Fabry–Perot resonances visible in the transmission spectrum of the device, obtained using a microspectrophotometer. The gap becomes slightly smaller

with increasing voltage because of deformation of the membrane and the nanowires by electrostatic forces, resulting in about 5% reduction of the gap between the effective (average) nanowire position and the back-plane at 18 V. The whole structure transmits between 12% and 58% of incident power in the 1370–1750 nm spectral range.

**Azimuth Rotation and Ellipticity Measurements:** The beam from a supercontinuum laser source was passed through an acousto-optical tunable filter to select wavelengths in the 1360–1750 nm range (with about  $\pm 5$  nm bandwidth). A polarizer and superachromatic half-wave plate were used to set the linear polarization state incident on the metamaterial device. The beam of less than 4 mm diameter was focused onto the sample by a 10 $\times$  microscope objective, resulting in a maximum angle of incidence onto the sample of less than 5°. Another 10 $\times$  objective was used to collimate the transmitted beam, and a polarimeter was used to quantify its polarization state (averaged over 100 repeated measurement cycles, each with a 30 ms integration time). A static bias of 0–18 V was applied between the metamaterial (gold layer) and the ITO back-plane using a DC power supply.

**Separation of Optical Activity and Optical Anisotropy:** Circular birefringence  $\Delta\varphi$  is evaluated as the  $\varphi_n$ -independent (average) component of polarization azimuth rotation, where  $\varphi_n$  is the polarization azimuth of the incident linearly polarized laser beam. Circular dichroism  $\Delta\zeta$  is correspondingly evaluated as the  $\varphi_n$ -independent (average) component of the ellipticity angle. A more detailed description of the method for separation of optical activity and optical anisotropy can be found in refs. [8,12,33,38].

## Supporting Information

Supporting Information is available from the Wiley Online Library or from the authors.

## Acknowledgements

This work was supported by the Engineering and Physical Sciences Research Council, UK (Grant No. EP/M009122/1), the MOE Singapore (Grant No. MOE2016-T3-1-006), and the China Scholarship Council (CSC No. 201706120205). Q.Z. would like to acknowledge constructive discussions with Dr. Artemios Karvounis during preparations for this work.

## Conflict of Interest

The authors declare no conflict of interest.

## Data Availability Statement

The data that support the findings of this study are openly available in the University of Southampton ePrints research repository at <https://doi.org/10.5258/SOTON/D1382>. (The statement has been added in September 2021, after initial online publication.)

## Keywords

chirality, electrogyration, electro-optic effect, metamaterials, nanoelectromechanical systems, optical activity

Received: October 21, 2020

Revised: November 17, 2020

Published online: December 16, 2020

[1] H. Futama, R. Pepinsky, *J. Phys. Soc. Jpn.* **1962**, *17*, 725.

[2] K. Aizu, *Phys. Rev.* **1964**, *133*, A1584.

- [3] I. S. Zheludev, *Kristallografiya* **1964**, 9, 501; English translation: *Sov. Phys. Crystallogr.* **1965**, 9, 418.
- [4] I. S. Zheludev, O. G. Vlokh, *Proc. Indian Acad. Sci. Chem. Sci.* **1983**, 92, 421.
- [5] O. G. Vlokh, *Ukr. Fiz. Zhurn.* **1970**, 15, 758.
- [6] O. G. Vlokh, R. O. Vlokh, *Opt. Photonics News* **2009**, 20, 34.
- [7] Y. Svirko, N. I. Zheludev, M. Osipov, *Appl. Phys. Lett.* **2001**, 78, 498.
- [8] E. Plum, V. A. Fedotov, A. S. Schwanecke, N. I. Zheludev, Y. Chen, *Appl. Phys. Lett.* **2007**, 90, 223113.
- [9] N. Liu, H. Liu, S. Zhu, H. Giessen, *Nat. Photonics* **2009**, 3, 157.
- [10] E. Plum, J. Zhou, J. Dong, V. A. Fedotov, T. Koschny, C. M. Soukoulis, N. I. Zheludev, *Phys. Rev. B* **2009**, 79, 035407.
- [11] S. Zhang, Y.-S. Park, J. Li, X. Lu, W. Zhang, X. Zhang, *Phys. Rev. Lett.* **2009**, 102, 023901.
- [12] Y. Cui, L. Kang, S. Lan, S. Rodrigues, W. Cai, *Nano Lett.* **2014**, 14, 1021.
- [13] M. Esposito, V. Tasco, F. Todisco, M. Cuscuná, A. Benedetti, D. Sanvitto, A. Passaseo, *Nat. Commun.* **2015**, 6, 6484.
- [14] M. Hentschel, M. Schäferling, X. Duan, H. Giessen, N. Liu, *Sci. Adv.* **2017**, 3, e1602735.
- [15] I. Fernandez-Corbaton, C. Rockstuhl, P. Ziemke, P. Gumbsch, A. Albiez, R. Schwaiger, T. Frenzel, M. Kadic, M. Wegener, *Adv. Mater.* **2019**, 31, 1807742.
- [16] T. Kan, A. Isozaki, N. Kanda, N. Nemoto, K. Konishi, H. Takahashi, M. Kuwata-Gonokami, K. Matsumoto, I. Shimoyama, *Nat. Commun.* **2015**, 6, 8422.
- [17] T. Kan, A. Isozaki, N. Kanda, N. Nemoto, K. Konishi, M. Kuwata-Gonokami, K. Matsumoto, I. Shimoyama, *Appl. Phys. Lett.* **2013**, 102, 221906.
- [18] L. Cong, P. Pitchappa, N. Wang, R. Singh, *Research* **2019**, 2019, 7084251.
- [19] M. Liu, Q. Xu, X. Chen, E. Plum, H. Li, X. Zhang, C. Zhang, C. Zou, J. Han, W. Zhang, *Sci. Rep.* **2019**, 9, 4097.
- [20] W. J. Choi, G. Cheng, Z. Huang, S. Zhang, T. B. Norris, N. A. Kotov, *Nat. Mater.* **2019**, 18, 820.
- [21] M. Kuwata-Gonokami, N. Saito, Y. Ino, M. Kauranen, K. Jefimovs, T. Vallius, J. Turunen, Y. Svirko, *Phys. Rev. Lett.* **2005**, 95, 227401.
- [22] N. I. Zheludev, E. Plum, *Nat. Nanotechnol.* **2016**, 11, 16.
- [23] H. Tao, A. C. Strikwerda, K. Fan, W. J. Padilla, X. Zhang, R. D. Averitt, *Phys. Rev. Lett.* **2009**, 103, 147401.
- [24] M. Lapine, D. Powell, M. Gorkunov, I. Shadrivov, R. Marqués, Y. S. Kivshar, *Appl. Phys. Lett.* **2009**, 95, 084105.
- [25] J. Y. Ou, E. Plum, L. Jiang, N. I. Zheludev, *Nano Lett.* **2011**, 11, 2142.
- [26] J. Y. Ou, E. Plum, J. Zhang, N. I. Zheludev, *Nat. Nanotechnol.* **2013**, 8, 252.
- [27] J. Valente, J. Y. Ou, E. Plum, I. J. Youngs, N. I. Zheludev, *Nat. Commun.* **2015**, 6, 7021.
- [28] J. Y. Ou, E. Plum, J. Zhang, N. I. Zheludev, *Adv. Mater.* **2016**, 28, 729.
- [29] M. Lapine, I. V. Shadrivov, D. A. Powell, Y. S. Kivshar, *Nat. Mater.* **2012**, 11, 30.
- [30] W. Zhu, Q. Song, L. Yan, W. Zhang, P. C. Wu, L. K. Chin, H. Cai, D. P. Tsai, Z. X. Shen, T. W. Deng, S. K. Ting, Y. Gu, G. Q. Lo, D. L. Kwong, Z. C. Yang, R. Huang, A.-Q. Liu, N. I. Zheludev, *Adv. Mater.* **2015**, 27, 4739.
- [31] I. M. Pryce, K. Aydin, Y. A. Kelaita, R. M. Briggs, H. A. Atwater, *Nano Lett.* **2010**, 10, 4222.
- [32] T. Shimura, T. Kinoshita, Y. Koto, N. Umeda, K. Iwami, *Appl. Phys. Lett.* **2018**, 113, 171905.
- [33] Y. P. Svirko, N. I. Zheludev, *Polarization of Light in Nonlinear Optics*, Wiley, New York **1998**.
- [34] H. Zhu, F. Yi, E. Cubukcu, *Nat. Photonics* **2016**, 10, 709.
- [35] P. Cencillo-Abad, J. Y. Ou, E. Plum, N. I. Zheludev, *Sci. Rep.* **2017**, 7, 5405.
- [36] D. R. Smith, S. Schultz, P. Markoš, C. M. Soukoulis, *Phys. Rev. B* **2002**, 65, 195104.
- [37] S. A. Akhmanov, B. V. Zhdanov, N. I. Zheludev, A. I. Kovrigin, V. I. Kuznetsov, *JETP Lett.* **1979**, 29, 264.
- [38] M. Ren, E. Plum, J. Xu, N. I. Zheludev, *Nat. Commun.* **2012**, 3, 833.
- [39] I. V. Shadrivov, V. A. Fedotov, D. A. Powell, Y. S. Kivshar, N. I. Zheludev, *New J. Phys.* **2011**, 13, 033025.